Available online at www.sciencedirect.com
SCIENCE DIRECT®
Journal of Solid State Chemistry 178 (2005) 1903–1914
JOURNAL OF SOLID STATE CHEMISTRY
www.elsevier.com/locate/jssc

A universally applicable composite modulated structure approach to ordered $Ba_xM_yTi_{8-y}O_{16}$ hollandite-type solid solutions

Melody L. Carter[a,b,*], Ray L. Withers[c]

[a]*Australian Nuclear Science and Technology Organisation, New Illawarra Road, Lucas Heights, NSW 2234, Australia*
[b]*School of Chemistry, The University of Sydney, Sydney, NSW 2006, Australia*
[c]*Research School of Chemistry, Australian National University, Canberra, ACT 0200, Australia*

Received 17 January 2005; received in revised form 24 March 2005; accepted 27 March 2005
Available online 26 April 2005

Abstract

A wide range of barium titanate hollandites of the form $Ba_x^{2+}M_x^{2+}Ti_{8-x}^{4+}O_{16}$ ($M = Zn$, Co, Mg, Fe and Mn) and $Ba_x^{2+}M_{2x}^{3+}Ti_{8-2x}^{4+}O_{16}$ ($M = Fe$) with nominal x ranging from 1.0 to 1.4 have been synthesized and examined to investigate the solid solution range and the nature of the ordering of the Ba ions. Electron diffraction studies confirm that the barium titanate hollandites are composite modulated single phase solid solutions made up of mutually incommensurable (along **b**) framework and Ba ion sub-structures. The overall superspace group symmetry was found to be $I'2/m(0,\frac{x}{2},0)1$. The symbol I' here refers to the superspace centering operation $\{x_1+\frac{1}{2},\ x_2+\frac{1}{2},\ x_3+\frac{1}{2},\ x_4+\frac{1}{2}\}$ (see below). Both the framework and the Ba sub-structures have the same $I2/m$ average structure space group symmetry. The solid solution ranges for the hollandites were calculated from the positions of well-defined superlattice peaks in X-ray diffraction patterns. The effect of cooling rate on Ba ion ordering is also examined.

Keywords: Hollandite; Electron diffraction; Composite modulated structure; Solid solution range

1. Introduction

The crystal structure of the mineral hollandite $Ba_xMn_8O_{16}$ was first reported by Byström and Byström [1] in 1950 and since then a rather large number of additional hollandite-type compounds have been synthesized and studied. The stoichiometry of all these compounds can be represented by the general formula $A_xB_8O_{16}$ ($1<x<2$) where the A cation may be monovalent (Na, K, Rb, Cs, Tl), divalent (Sr, Ba and Pb), or a mixture of both, and a range of cations with valences in the range $+2$ to $+5$ may occupy the B site. (Cations found in the smaller B site of hollandites include Zn, Cr, Mn, Fe, Co, Al, Ga, Rh, Ru, Ti and Mo.)

The basis of the hollandite structure type is a (usually) well-defined BO_2 octahedral framework sub-structure into the square tunnel interstices of which are located the A cations. This BO_2 octahedral framework sub-structure is formed by corner-sharing columns of double edge-sharing octahedra enclosing an array of two-by-two square tunnels running parallel to the short axis of the structure (see Fig. 1). It usually has tetragonal $I4/m$ space group symmetry with the tunnel axis running along the **c** direction. In many cases, however, this space group symmetry is reduced to monoclinic $I2/m$ (with the tunnel axis now running along the crystallographically unique **b** direction) and with the β angle slightly greater than 90°. This slight monoclinic distortion occurs when the tunnel ions are not large enough to support the tunnel walls and occurs via a hinged rotation mechanism around the corner-connected linkages (see e.g., Ref. [2]).

As a general rule, hollandites with large A ions and small B ions are tetragonal whereas those with small A

*Corresponding author. Australian Nuclear Science and Technology Organisation, New Illawarra Road, Lucas Heights, NSW 2234, Australia. Fax: +61 2 9543 7179.
E-mail address: mlc@ansto.gov.au (M.L. Carter).

0022-4596/$ - see front matter © 2005 Elsevier Inc. All rights reserved.
doi:10.1016/j.jssc.2005.03.040

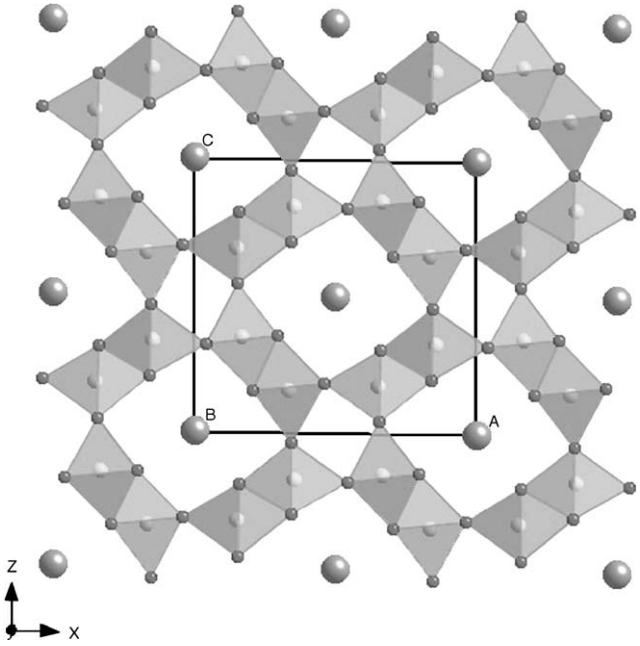

Fig. 1. A projection of the average hollandite structure along the b, or tunnel, direction. Linked BO_6 octahedra containing B cations form the tunnel framework. The A ions occupy tunnel sites.

ions and large B ions are monoclinic (at room temperature). Post et al. [3] proposed that $r_B/r_A = 0.48$ corresponds to the approximate tetragonal/monoclinic boundary (at room temperature), where r_B is the average ionic radius of the six-coordinate B cation/s and r_A that of the eight-coordinate A cation [4]. Hollandites in which $r_B/r_A < 0.48$ are tetragonal and those with a larger ratio are monoclinic.

In addition to the strong sharp Bragg reflections arising from this well-defined BO_2 octahedral framework sub-structure, the reciprocal lattices of hollandites invariably display one or other of two extreme types of additional scattering. The first type of additional scattering takes the form of sheets of diffuse intensity normal to c^* (in the case of tetragonal hollandites) or b^* (in the case of monoclinic hollandites). Such diffuse sheets have been observed in both natural as well as synthetic hollandites (see e.g., Figs. 2a and 3a) and imply long-range ordering of the interstitial A cations along the tunnel directions but with little or no transverse correlation from tunnel to tunnel.

The other extreme type of additional scattering takes the form of sharp additional satellite reflections (see e.g., Figs. 2b and 3b). Intermediate cases between these two extreme types of additional scattering have, however, also been reported [5–17]. In this paper we focus largely on the latter, long-range ordered type of additional scattering, in particular on the $Ba_xM_yTi_{8-y}O_{16}$ family of hollandites which all exhibit sharp (in general incommensurate) satellite reflections in addition to the strong

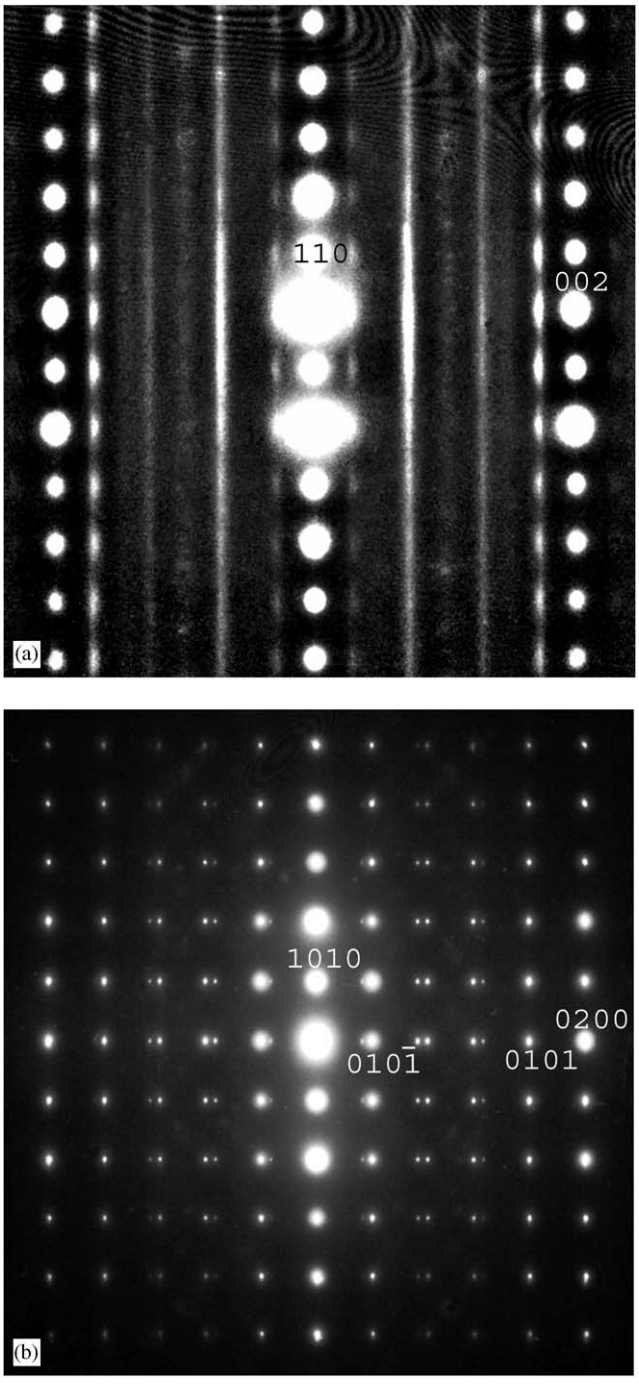

Fig. 2. (a) A typical $[1\bar{1}0]$ zone axis EDP of $Cs_{1.5}Zn_{0.75}Ti_{7.25}O_{16}$ (nominal composition). (b) A typical $[10\bar{1}]$ zone axis EDP of $Ba_{1.16}Zn_{1.16}Ti_{6.84}O_{16}$ (nominal composition).

Bragg reflections of the underlying BO_2 octahedral framework sub-structure.

It is generally agreed that these usually weak, additional satellite reflections are due to the ordered arrangement of the A cations within the hollandite tunnels (the sharper the satellite reflections, the greater the degree of cation ordering). Despite the weakness of

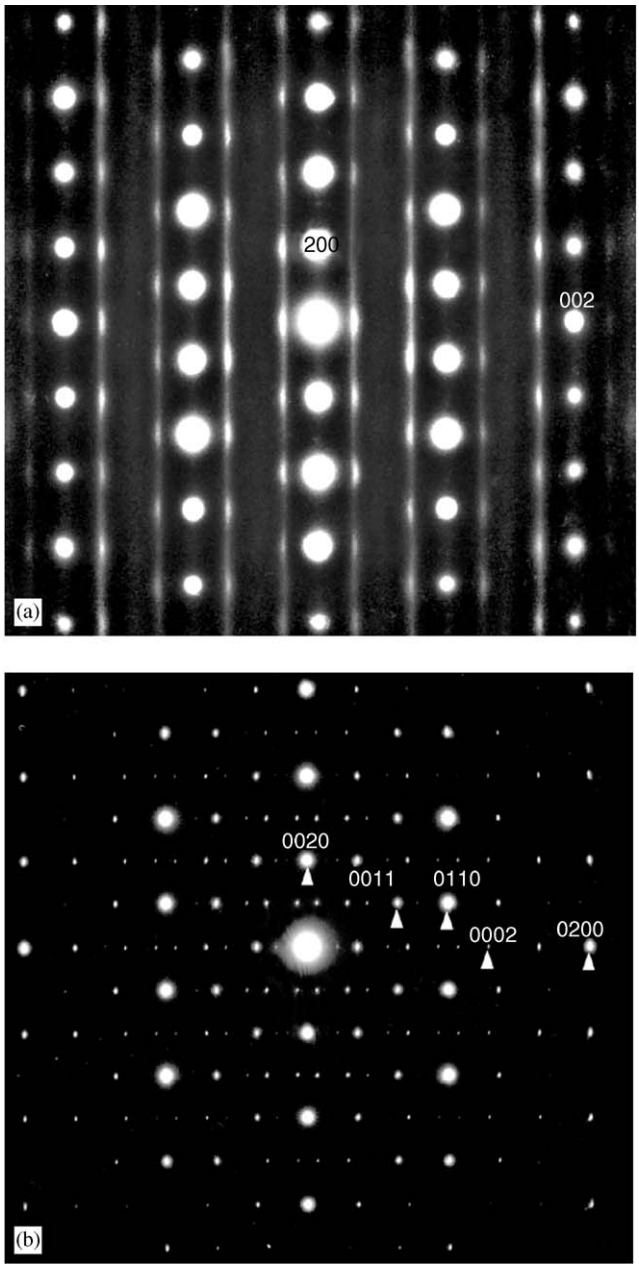

Fig. 3. (a) A typical [110] zone axis EDP of $Cs_{1.5}Zn_{0.75}Ti_{7.25}O_{16}$ (nominal composition). (b) A typical [100] zone axis EDP of $Ba_{1.30}Zn_{1.30}Ti_{6.70}O_{16}$ (nominal composition).

these additional satellite reflections, they have been detected in powder X-ray diffraction patterns [18–21] as well as in electron diffraction patterns (EDPs). The satellite peaks are often well resolved, as e.g., in the case of the $Ba_x(Mg,Ti)_8O_{16}$ hollandites, but are sometimes consistently diffuse despite long annealing times to encourage ordering [19].

Given that there are formally $\frac{x}{2}$ Ba cations and $(1-\frac{x}{2})$ Ba vacancies per framework sub-structure repeat along the tunnel directions, Mijlhoff et al. [13] attributed the existence of these weak incommensurate satellite reflections to a simple Ba vacancy ordering model. They proposed that the ordering of vacant and occupied tunnel sites within the host BO_2 octahedral framework sub-structure occurs over a superstructure period equivalent to a multiplicity $(m)\times c$ (the period of the host BO_2 octahedral framework sub-structure) (or $(m)\times b$ in the case of monoclinic hollandites). The multiplicity m was defined as "...the ratio between the repeat period of the modulation and the basic lattice period..." [13], i.e., $m=\frac{1}{2}(|[0200]*|/|[010\bar{1}]*|)$ (see e.g., Fig. 3b) $=b_f*/(b_f*-b_{Ba}*)$ (subscript f for octahedral framework sub-structure and subscript Ba for the Ba ion sub-structure)$=2/(2-x)$ with respect to our indexation scheme [22] and writing the stoichiometry in the form $A_xB_8O_{16}$. (Note that Mijlhoff et al. [13] write the overall stoichiometry as $A_xB_4O_8$ or $A_{2x}B_8O_{16}$, i.e., x_M (subscript M for Mijlhoff) $=x/2$).) To add to the confusion, Bursill and Grzinic [10] as well as Cheary and Squadrito [19,20] use a multiplicity, m_{BG}, double that of Mijlhoff et al. [13], i.e., $m_{BG}=2m$.

Mijlhoff et al. [13] also developed a model in which vacant and occupied sites were arranged so as to avoid consecutive vacant sites and proposed the relationship $x_M=1-(1/m)$ (equivalently $x=2[1-(1/m)]$ or $2[1-(2/mBG)]$) between Ba content x and superstructure periodicity m. (Strictly, however, the requirement that consecutive vacant sites should be avoided does not give rise to an equality but only to an upper or lower bound on the multiplicity as follows: $1-x_M\leqslant 1/m\leqslant x_M$ for $x_M>\frac{1}{2}$ and $x_M\leqslant 1/m\leqslant 1-x_M$ for $x_M<\frac{1}{2}$, i.e., the approach of Mijlhoff et al. [13] does not lead to a necessary relationship between composition x and the positioning of the satellite reflections.) The relationship proposed by Mijlhoff et al. [13], $x_M=1-(1/m)$, has subsequently been used by most workers to calculate the A site content (see e.g., Eq. (1) of Ref. [19], etc.).

More recently, Carter and Withers [22] studied the barium nickel hollandite ($Ba_xNi_xTi_{8-x}O_{16}$) system and concluded that it is best described as a (3+1)-d composite modulated single phase solid solution (see e.g., Refs. [23–25]) made up of mutually incommensurable (along **b**), $I2/m$ octahedral framework (subscript f) and $I2/m$ Ba ion (subscript Ba) sub-structures. Each sub-structure is modulated by the other sub-structure, with the relevant (in general incommensurate) primary modulation wave-vector characteristic of each sub-structure corresponding to the **b*** lattice vector of the other sub-structure. Indexation in Ref. [22] as well as in Figs. 2b and 3b is thus with respect to the basis vector set $M^*=\{\mathbf{a}^*, \mathbf{b}_f^*, \mathbf{c}^*, \mathbf{q}=\mathbf{b}_{Ba}^*\}$. The relevant incommensurate primary modulation wave-vector of the framework sub-structure is thus given by $\mathbf{q}^i=\mathbf{b}_{Ba}^*$. (Note that it is standard convention (see p. 804 of Ref. [25]) when a primitive primary modulation wave-vector, $\mathbf{q}_p$, has a rational as well as an irrational component, as in the current case where

$\mathbf{q_p} = [011]_{Ba}^* = [0011]^* = \mathbf{c}^* + \mathbf{b}_{Ba}^*$ (see e.g., Fig. 2b), to remove the rational $\mathbf{c}^*$ component and choose the irrational $\mathbf{q}^i$ component as the new modulation wavevector $\mathbf{q}$).

The magnitude of this primary modulation wavevector, when measured directly from EDPs was shown to act as a 'chemical ruler' in that it was directly related to overall composition and given by $\frac{x}{2}$. (Given that there are formally $\frac{x}{2}$ Ba cations per framework sub-structure repeat along the tunnel direction (see Fig. 1), it is clear that $\mathbf{b}_f$ must equal $\frac{x}{2}\,\mathbf{b}_{Ba}$ and hence $\mathbf{q} = \mathbf{b}_{Ba}^*$ necessarily equals $\frac{x}{2}\mathbf{b}_f^*$.) In this composite modulated structure approach, there is thus a direct and necessary relationship between composition and the positioning of 'satellite reflections'. The only observed systematic extinction condition when indexation was carried out with respect to the above basis vector set was that $hklm$ reflections are allowed only if $h+k+l+m$ is even, requiring the existence of the superspace centering operation $I' = \{x_1 + \frac{1}{2},\ x_2 + \frac{1}{2},\ x_3 + \frac{1}{2},\ x_4 + \frac{1}{2}\}$. The overall superspace group symmetry was found to be $I'2/m(0,\frac{x}{2},0)1$. The relevant superspace generating operations are given in Ref. [22].

In this work, we examine a wide range of long-range ordered Ba titanate hollandites and find that the composite modulated structure approach just described provides a universal framework for understanding the crystallography of all such materials. The solid solution ranges for the hollandite systems studied are calculated using X-ray diffraction data.

2. Experimental

Hollandite samples with nominal compositions $Ba_xM_x^{2+}Ti_{8-x}O_{16}$ (M = Zn, Co, Mg, Fe and Mn) and $Ba_xM_{2x}^{3+}Ti_{8-2x}O_{16}$ (M = Fe) over the composition range $x = 1.0$–1.4 as well as $Cs_{1.5}Zn_{0.75}Ti_{7.25}O_{16}$ have been synthesized and studied. Note that earlier work by Carter et al. [26] showed that Mn-containing hollandites did not contain Mn^{3+} when processed in air so only hollandites containing Mn^{2+} were synthesized in this study.

The various samples were produced by the alkoxide route [27]. This method involves mixing the appropriate molar quantities of titanium (IV) isopropoxide dissolved in ethanol with an aqueous solution of Ba and M nitrates, whilst continuously stirring. This mixture was then heated to dryness at ~110 °C. The dry product was calcined in air for 2 h at 750 °C and then wet ball milled. The resultant samples were then sintered in air or argon (for $M = Fe^{2+}$ and Mn^{2+}) for 20 h at 1300 °C and cooled at 5 °C/min. The Fe^{3+} samples sintered in air were cooled at both 5 °C/min and 3 °C/h.

The alkoxide route is an excellent method for preparing intimately mixed precursor material which in turn enables lower-temperature firing. It does, however, have a slight drawback when making hollandites in that small amounts of secondary phases in addition to the desired equilibrium phase are often formed as a result of kinetic factors so that the resultant composition of the majority hollandite phase is sometimes slightly different from the nominal composition. Microscopic compositional analysis of the hollandite is thus usually required.

A JEOL JSM6400 scanning electron microscope (SEM) equipped with a Noran Voyager energy-dispersive spectroscopy system (EDS) was operated at 15 keV for microstructural analysis work. A Philips EM 430 microscope operating at 300 kV was used for the electron diffraction work.

Laboratory X-ray diffraction was performed with an Xpert unit and Cu$K\alpha$ radiation using a nickel filter and 10 mm mask. Samples were rotated at 1/2 a rotation per second and the samples were measured between 10° and 65°, with a step size of 0.0167° in a continuous scan mode with a counting time of 400 s. Lattice parameters were calculated using Jade 6.0 software, Jade 6 uses a full-profile fit. The pattern background was fitted using a cubic spline with the automatic threshold function in Jade 6. Peaks were fitted and refined using Pearson VII peak shapes and the $K\alpha_2$ peaks were not subtracted (Jade uses a doublet for $K\alpha - K\alpha_2$ peak fitting). A zero line correction was used. The lattice parameters were calculated using $I4/m$ space group symmetry for the tetragonal samples and $I2/m$ space group symmetry (b unique) for the monoclinic hollandite samples.

To determine the experimental compositional solid solution range of the various hollandite systems investigated, the method of Carter and Withers [22] was used. This involves determining the overall Ba content from measured satellite peak positions. To do this, it was first of all necessary to determine the lattice parameters a, b_f, c and β of the octahedral framework sub-structure. Following this, these parameters were then held fixed (along with the zero line correction for the framework) and a b_{Ba} cell parameter for the Ba ion sub-structure obtained by fitting all the additional satellite peaks in the XRD patterns. Finally, the Ba content, x, was calculated using the formula $x = 2b$ (framework sub-cell)/b (Ba sub-cell).

3. Results

3.1. SEM

All synthesized samples in the $Ba_xM_x^{2+}Ti_{8-x}O_{16}$ (M = Zn, Co, Mg, Fe and Mn) and $Ba_xM_{2x}^{3+}Ti_{8-2x}O_{16}$ (M = Fe) systems were examined via EDS in the SEM (prior to diffraction studies) to determine phase composition. The hollandite solid solution phase was

Table 1
Minor phases present in the $Ba_xM_x^{2+}Ti_{8-x}O_{16}$ (M = Zn, Co, Mg, Fe and Mn), $Ba_xM_{2x}^{3+}Ti_{8-2x}O_{16}$ (M = Fe) samples examined

Composition	Nominal Ba content (x)	Minor phases
$Ba_xZn_xTi_{8-x}O_{16}$	$x \leqslant 1.16$	Rutile
	$1.16 < x < 1.22$	Near single phase hollandite
	$1.22 < x < 1.4$	$BaTi_5O_{11}$ and $Ba_3Zn_7Ti_{12}O_{34}$
$Ba_xCo_xTi_{8-x}O_{16}$	$1.10 < x < 1.16$	Rutile and a small amount of $BaTi_5O_{11}$
	$1.16 \leqslant x \leqslant 1.28$	Near single phase hollandite
	$1.28 < x \leqslant 1.40$	of $BaTi_5O_{11}$ and an unidentified Ba/Co/titanate
$Ba_xMg_xTi_{8-x}O_{16}$	$1.10 < x < 1.16$	Rutile
	$1.16 \leqslant x \leqslant 1.28$	Near single phase hollandite with small amount of $BaTi_5O_{11}$ (<0.5%)
	$1.28 < x \leqslant 1.40$	$BaTi_5O_{11}$
$Ba_xMn_xTi_{8-x}O_{16}$	$1.10 < x < 1.14$	Rutile and a small amount of $BaTi_5O_{11}$
	$1.14 \leqslant x \leqslant 1.24$	Near single phase hollandite with a small amount of $BaTi_5O_{11}$ (<1.0%)
	$1.24 < x < 1.40$	$BaTi_5O_{11}$ and $MnTiO_3$
$Ba_xFe_{2x}Ti_{8-2x}O_{16}$ (Fe^{3+})	$x = 1.0$	Rutile
	$1.10 \leqslant x \leqslant 1.30$	Near single phase hollandite
	$1.30 < x \leqslant 1.40$	$BaFe_4Ti_2O_{11}$ and $Ba_2Fe_2Ti_4O_{13}$
$Ba_xFe_xTi_{8-x}O_{16}$ (Fe^{2+})	$x = 1.0$	$Fe_2Ti_5O_{12}$
	$1.10 \leqslant x \leqslant 1.30$	Near single phase hollandite
	$1.30 < x \leqslant 1.40$	An unidentified Ba/Fe/titanate

always found to be by far the majority phase in all cases. Minor amounts of secondary phases were, however, often detected. Table 1 lists the minor phases present in the samples examined. Note that the amount of rutile detected decreased to near zero as x approached the minimum Ba content for the hollandites studied. When the maximum Ba content for the hollandite solid solution phase was exceeded, the amount of other secondary phases detected increased with increasing Ba content.

3.2. TEM

EDPs of the various hollandite-type samples were found to be quite reproducible from grain to grain and entirely consistent with previously reported EDPs of the $Ba_xNi_xTi_{8-x}O_{16}$ hollandite system ([22]). Fig. 2b, e.g., shows a typical [10$\bar{1}$] zone axis EDP of $Ba_{1.16}Zn_{1.16}Ti_{6.84}O_{16}$ (nominal composition) while Fig. 3b shows a typical [100] zone axis EDP of $Ba_{1.30}Zn_{1.30}Ti_{6.70}O_{16}$ (nominal composition) (cf. with the equivalent zone axis EDPs shown in e.g., Figs. 2–4 of Carter and Withers [22]). In addition to the strong Bragg reflections corresponding to the underlying average B_8O_{16} framework sub-structure (those reflections labelled $hkl0$ in Figs. 2b and 3b), note the presence of additional sharp incommensurate satellite reflections running along the $\mathbf{b}_f^*$ (f for framework) direction of reciprocal space. Note also that the same systematic extinction condition as occurred for the Ni hollandite, namely $F(hklm)$ is zero unless $h+k+l+m$ is even, is also characteristic of the Zn and other hollandites (see Figs. 2b and 3b). Thus the overall superspace group symmetry was confirmed to be $I'2/m(0,\frac{x}{2},0)1$, as for the Ni hollandites. Both the framework and the Ba sub-structures thus have the same $I2/m$ average structure space group symmetry [22].

3.3. Solid solution ranges from XRD data

3.3.1. $Ba_xZn_xTi_{8-x}O_{16}$ $Ba_xCo_xTi_{8-x}O_{16}$, $Ba_xMg_xTi_{8-x}O_{16}$ and $Ba_xMn_xTi_{8-x}O_{16}$

Laboratory XRD data showed the octahedral framework sub-structure of all samples to be monoclinic with a monoclinic β angle slightly larger than 90°. β was found to deviate further from 90° with increasing Ba content (as can be deduced from the increased splitting of the most intense framework sub-structure peaks with increasing Ba content—see Fig. 4). In addition to the reflections of the monoclinic framework sub-structure, however, additional reflections arising from the Ba sub-structure (and from cross-term combinations of the reciprocal lattice reflections of both parent sub-structure reciprocal lattices) are also always present (see e.g., Figs. 4 and 5). These weak additional satellite reflections are always quite sharp and move systematically with changing Ba composition x. Weak peaks from secondary phases were also clearly present when the abundance of the secondary phase was greater than approximately 5%.

From the similarity of the electron, the SEM and XRD data presented here to that reported for the $Ba_xNi_xTi_{8-x}O_{16}$ system by Carter and Withers [22], it is clear that the $Ba_xZn_xTi_{8-x}O_{16}$, $Ba_xCo_xTi_{8-x}O_{16}$, $Ba_xMg_xTi_{8-x}O_{16}$ and $Ba_xMn_xTi_{8-x}O_{16}$ systems also

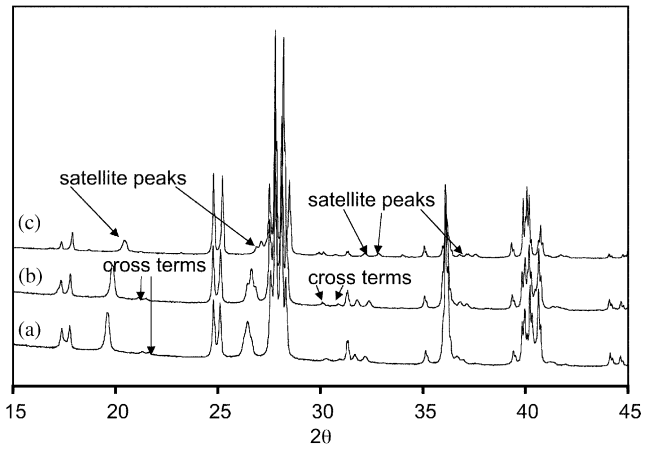

Fig. 4. XRD patterns of $Ba_xZn_xTi_{8-x}O_{16}$ with nominal composition of (a) $x = 1.16$, (b) $x = 1.20$ and (c) $x = 1.24$.

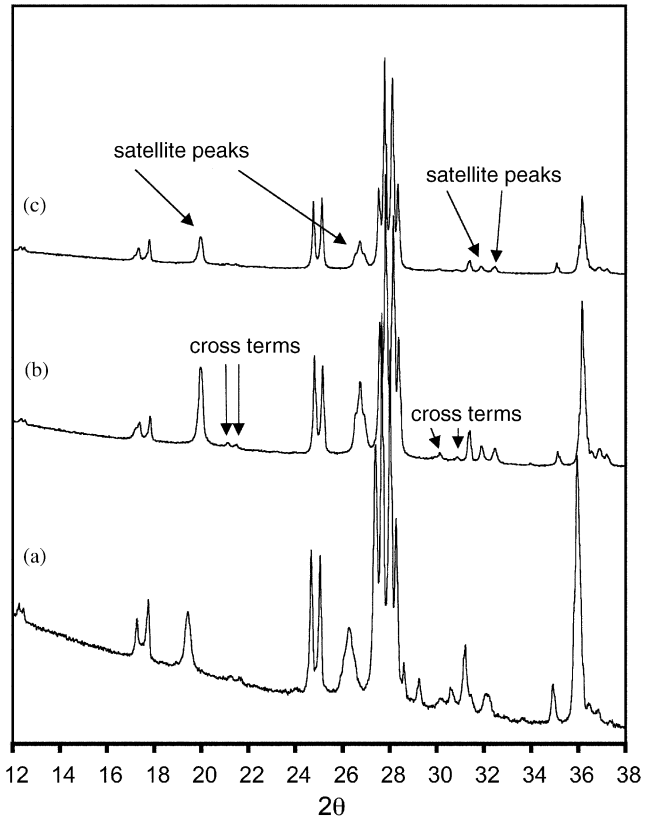

Fig. 5. XRD patterns of (a) $Ba_xMn_xTi_{8-x}O_{16}$, (b) $Ba_xCo_xTi_{8-x}O_{16}$ and (c) $Ba_xMg_xTi_{8-x}O_{16}$, for $x = 1.18$.

behave as composite modulated single phase solid solutions.

Table 2 lists the refined lattice parameters of the octahedral framework sub-structure of the $Ba_xZn_xTi_{8-x}O_{16}$ hollandite solid solution along with the calculated values of the composition x as a function of the nominal composition x. Note that the relatively slight deviation in calculated Ba content from the nominal Ba content is only to be expected due to the presence in all samples of minor amounts of secondary phases as discussed above. Note that the hollandite phase in samples with nominal compositions from $x = 1.20$ to 1.26 is essentially the same to within error suggesting that the high x, end-member composition occurs at $x \sim 1.24$. The calculated composition range for $M = Zn$ is thus from $1.174(2) \leqslant x \leqslant \sim 1.24$. Compositional analysis within the SEM showed all of these samples to contain secondary phases with the $x = 1.26$ sample containing the greatest amount of secondary phases.

Table 2
Lattice parameters determined for the framework sub-cell along with the calculated x values for a selection of $Ba_xZn_xTi_{8-x}O_{16}$ samples

Nominal x	a (Å)	b (Å)	c (Å)	β (°)	Calculated x
1.16	10.219(1)	2.978(1)	9.989(1)	90.72(2)	1.174(2)
1.18	10.232(1)	2.979(1)	9.973(2)	90.82(2)	1.194(2)
1.20	10.252(1)	2.982(1)	9.942(1)	90.98(2)	1.245(2)
1.22	10.251(1)	2.982(1)	9.942(1)	90.98(2)	1.236(2)
1.24	10.252(1)	2.982(1)	9.939(1)	91.99(2)	1.240(2)
1.26	10.251(1)	2.981(1)	9.942(1)	91.98(2)	1.237(2)

Errors in parentheses.

Table 3
Lattice parameters determined for the framework sub-cell along with the calculated minimum and maximum Ba occupancy for $Ba_xCo_xTi_{8-x}O_{16}$, $Ba_xMg_xTi_{8-x}O_{16}$ and $Ba_xMn_xTi_{8-x}O_{16}$

Sample	a (Å)	b (Å)	c (Å)	β (°)	Calculated x
$Ba_xCo_xTi_{8-x}O_{16}$					
Minimum	10.200(1)	2.970(1)	10.005(1)	90.62(1)	1.164(2)
Maximum	10.262(1)	2.975(1)	9.912(2)	91.13(1)	1.301(2)
$Ba_xMg_xTi_{8-x}O_{16}$					
Minimum	10.178(1)	2.971(1)	10.010(1)	90.50(1)	1.147(2)
Maximum	10.254(1)	2.979(1)	9.921(1)	91.06(1)	1.296(2)
$Ba_xMn_xTi_{8-x}O_{16}$					
Minimum	10.279(1)	2.991(1)	10.001(1)	91.87(2)	1.168(2)
Maximum	10.313(1)	2.994(1)	9.942(1)	91.98(2)	1.234(2)

Errors in parentheses.

Table 3 lists the refined octahedral framework sub-structure lattice parameters along with the calculated value of the composition x for the solid solution end-members of the $Ba_xCo_xTi_{8-x}O_{16}$, $Ba_xMg_xTi_{8-x}O_{16}$ and $Ba_xMn_xTi_{8-x}O_{16}$ hollandite systems. The method described above was used to determine the minimum and maximum values of x for each set of samples, i.e., to obtain the Ba content of the solid solution end-members and hence the observed composition range. The maximum and minimum values for x (the solid solution range) also coincide with the maximum and minimum

Table 4
Lattice parameters determined for the framework sub-cell along with the calculated x values for a selection of samples in the slowly cooled $Ba_xFe_{2x}Ti_{8-2x}O_{16}$ and $Ba_xFe_xTi_{8-x}O_{16}$ systems

Sample	a (Å)	b (Å)	c (Å)	β (°)	Calculated x
$Ba_xFe_{2x}Ti_{8-2x}O_{16}$					Superlattice peaks too weak
$x = 1$ (tetragonal)	10.103(1)		2.970(1)		
$x = 1.2$	10.180(1)	2.973(1)	10.013(1)	90·53(2)	1.210(3)
$x = 1.3$	10.221(1)	2.977(1)	9.955(1)	90·86(2)	1.291(2)
$x = 1.4$	10.247(1)	2.981(1)	9.906(1)	91·10(2)	1.350(2)
$Ba_xFe_xTi_{8-x}O_{16}$					Superlattice peaks too weak
$x = 1$ (tetragonal)	10.139(1)		2.971(1)		
$x = 1.2$	10.225(1)	2.976(1)	10.018(1)	90·71(2)	1.251(3)
$x = 1.3$	10.287(1)	2.978(1)	9.934(1)	91·15(2)	1.309(2)
$x = 1.4$	10.287(1)	2.978(1)	9.933(1)	91·15(2)	1.306(2)

Errors in parentheses.

values of the framework sub-cell lattice parameters. Note that the composition range of the $M = Zn$ or Mn systems are significantly narrower than those of the $M = Co$ or Mg systems (see Tables 2 and 3).

As for the $M = Zn$ hollandite system, minor deviations in the calculated Ba content from the nominal Ba content is only to be expected due to the presence in all samples of minor amounts of secondary phases as discussed above (see also Table 1).

3.3.2. $Ba_xFe_{2x}Ti_{8-2x}O_{16}$ (Fe^{3+}) and $Ba_xFe_xTi_{8-x}O_{16}$ (Fe^{2+}) hollandites

As for the previous systems, all synthesized samples in these systems were also examined via EDS in the SEM (prior to diffraction studies) to determine phase composition. Table 4 lists the refined octahedral framework sub-structure lattice parameters along with the calculated value of the composition x as a function of nominal composition. The hollandite solid solution phase was again always found to be by far the majority phase in all cases. Minor secondary phases, however, were again also detected for each system.

Laboratory XRD data showed the framework substructure of the air processed, Fe^{3+}-containing $Ba_xFe_{2x}Ti_{8-2x}O_{16}$ system to be tetragonal when $x<1.17$ and monoclinic above $x\sim1.17$. Such a tetragonal to monoclinic transformation has been reported elsewhere [30]. The tetragonal samples cooled at 5 °C/min, however, showed only broad, very weak superlattice peaks that were too weak and broad to allow measurement of x. The monoclinic samples showed sharper superlattice peaks enabling measurement of composition x (see Table 4). The superlattice peaks, however, were definitely not as well defined as those in the $Ba_xCo_xTi_{8-x}O_{16}$, $Ba_xMg_xTi_{8-x}O_{16}$ and $Ba_xZn_xTi_{8-x}O_{16}$ systems.

Earlier work by Cheary et al. [18] showed the ordering of the Ba ions could be enhanced and thus the superlattice peaks sharpened by slow cooling. The

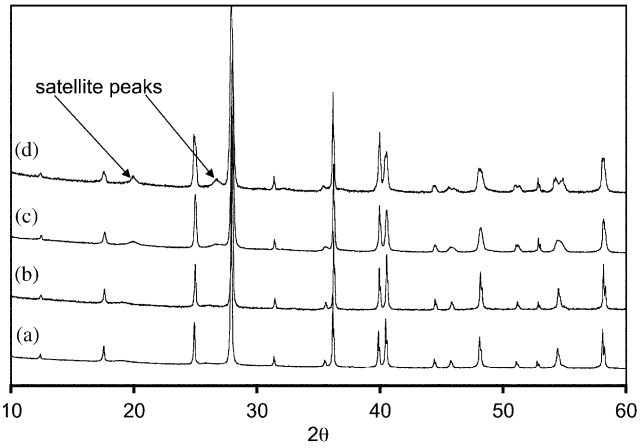

Fig. 6. XRD patterns of $Ba_xFe_{2x}Ti_{8-2x}O_{16}$ with nominal composition of (a) $x = 1.1$ cooled 5 °C/min, (b) $x = 1.1$ cooled 3 °C/h, (c) $x = 1.17$ cooled 5 °C/min, and (d) $x = 1.17$ cooled 3 °C/h.

$Ba_xFe_{2x}Ti_{8-2x}O_{16}$ hollandites were thus sintered and cooled from 1300 °C at 3 °C/h to see if the Ba arrangement might become more ordered. The XRD data, however, showed the superlattice peaks in the tetragonal samples to have changed very little for $x = 1.1$ and to have only slightly sharpened at 1.17 (see Fig. 6). The monoclinic samples cooled at the slower rate had slightly sharper superlattice peaks (see Fig. 7) but were still slightly broader than the Co, Zn, Mg and Mn hollandites. The same method as described above was again used to determine Ba content x and is given in Table 4. It should be noted that the different cooling rates used in this study did not change the central position of the superlattice peaks as also found in the work by Cheary et al. [19].

Laboratory XRD data showed the framework substructure of the argon processed, Fe^{2+}-containing $Ba_xFe_xTi_{8-x}O_{16}$ samples to be tetragonal when $x<1.2$ and monoclinic for $1.2<x<1.4$. As for the Fe^{2+}-containing hollandites, the tetragonal samples had very

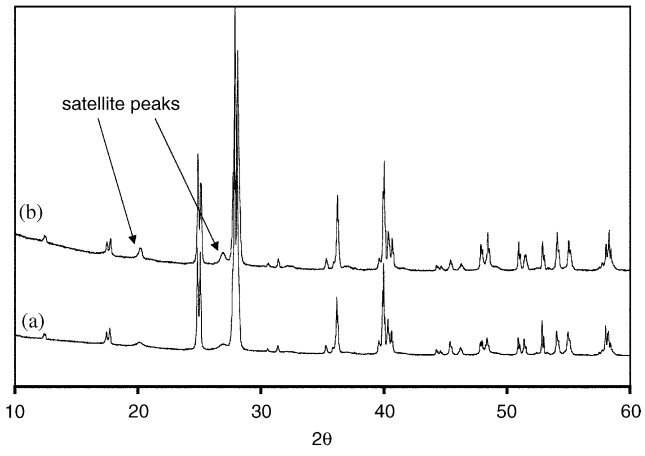

Fig. 7. XRD patterns of $Ba_xFe_{2x}Ti_{8-2x}O_{16}$ with nominal composition of (a) $x = 1.2$ cooled 5 °C/min and (b) $x = 1.2$ cooled 3 °C/h.

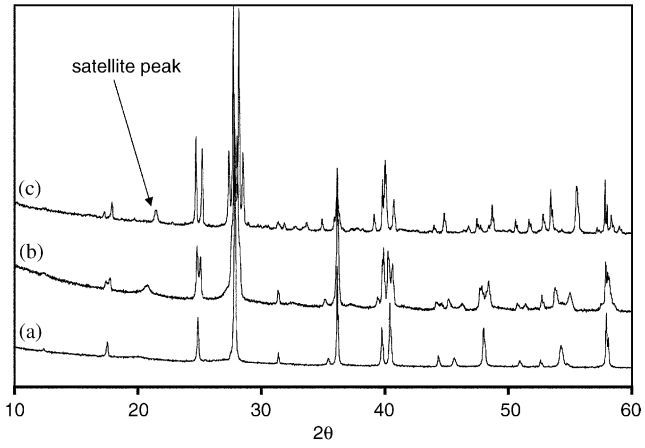

Fig. 8. XRD patterns of $Ba_xFe_xTi_{8-x}O_{16}$ with nominal composition of (a) $x = 1.1$ (b) $x = 1.2$ and (c) $x = 1.3$.

weak, broad satellite peaks. The monoclinic samples with $x > 1.2$, however, showed rather sharper peaks (see e.g., Fig. 8). Table 4 also lists the lattice parameters determined for the framework sub-cell along with the calculated x values for samples in this $Ba_xFe_xTi_{8-x}O_{16}$ system.

3.4. Quenching

In this study, we quenched selected hollandites to see if the three-dimensional ordering of the Ba ions could be removed. Fig. 9 shows the X-ray diffraction patterns of a $Ba_xCo_xTi_{8-x}O_{16}$ hollandite cooled at 5 °C/min (b) and quenched from 1200 °C to room temperature in less than 1 min (a). All but the strongest superlattice peaks have disappeared with the main superlattice peaks ($2\theta \sim 20°$ and 27°) becoming both weaker and broader.

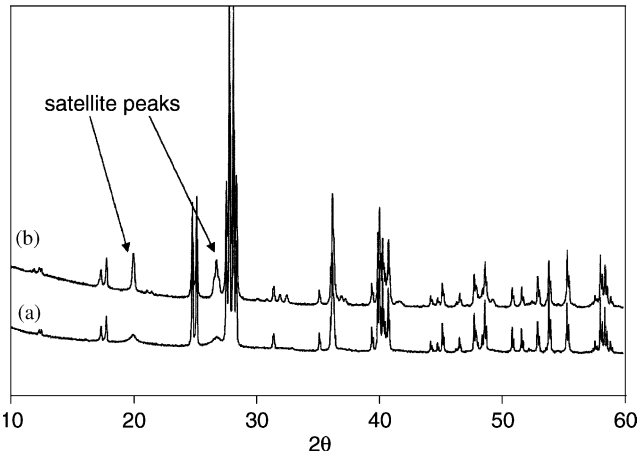

Fig. 9. XRD patterns of $Ba_xCo_xTi_{8-x}O_{16}$ (a) quenched, and (b) cooled at 5 °C/min.

4. Discussion

4.1. Solid solution ranges

The solid solution ranges found in this study were found to be significantly different for the various hollandites investigated (the composition range of the $M = Zn$ and Mn systems, e.g., have approximately half the extent of those of the $M = Co$ or Mg systems), although the Ba occupancy x was always found to be somewhere in the range from ~1.10 to ~1.35. There appears to be no obvious correlation between the size of the octahedral framework sub-cell and the extent of the solid solution range for the hollandite systems examined.

Roth et al. [28] most recently examined the ternary $BaO–ZnO–TiO_2$ system and reported it to contain four ternary phases, one of which is the $Ba_xZn_xTi_{8-x}O_{16}$ hollandite solid solution phase discussed above. They predicted it would be a continuous solid solution over a small range of x (see Fig. 17, Ref. [28]). The corresponding range, however, was not given. Our results (see Table 2) suggest that this range is from 1.174(2) to 1.245(2).

The solid solution range for the $Ba_xCo_xTi_{8-x}O_{16}$ hollandite solid solution (see Table 3) has been determined to run from $x = 1.164(2)$ to 1.301(2). Prior to this work, no reference to a $Ba_xCo_xTi_{8-x}O_{16}$ hollandite-type phase could be found in the literature.

The existence of a $Ba_xMg_xTi_{8-x}O_{16}$ hollandite-type phase was first mentioned by Dryden and Wadsley [5] who reported a tetragonal unit cell for it. It has since been studied by several other groups [5,10,19,20]. According to Bursill and Grzinic [10], e.g., $Ba_xMg_xTi_{8-x}O_{16}$ (and $Ba_xGa_{2x}Ti_{8-2x}O_{16}$) are stable over the composition range $x = 0.8–1.33$. These authors, however, also reported a superlattice periodicity of

$m_{BG} = 4.70$ for their $x = 0.8$ sample and $m_{BG} = 5.8-5.9$ for their $x = 1.33$ sample. Using the model developed by Mijlhoff et al. [13] where $x = 2(1-^{2}/_{m_{BG}})$, the Ba content in Bursill and Grzinic's hollandites [10] equates a range of x from 1.15 to 1.31–1.32 (and not all the way to 1.33). This is in reasonable agreement with the composition range for Ba content found in this study of $1.147(2) \leqslant x \leqslant 1.296(2)$.

Cheary and Squadrito [20] also examined the $Ba_xMg_xTi_{8-x}O_{16}$ hollandite system but this time using X-ray powder diffraction and Rietveld refinement of high-resolution neutron powder diffraction data. They reported the end member compositions to be $x = 1.14$ and 1.33, respectively, using their own method for determining Ba content as described below. The lattice parameters they found for their high x, end member composition, however, agree well with the results from our study suggesting that the apparent discrepancy in end-member composition is an artifact arising from the different measurement technique used.

Cheary and Squadrito [20] calculated overall Ba content from the position of a particular satellite peak in their XRD data near 20° 2θ (using Cu$K\alpha$ radiation). They indexed this peak as $(0k1)/(1k0)$ (in fact this peak consists of four separate overlapping peaks (see Ref. [22]) thereby introducing error into their calculations) and determined the magnitude of the parameter k as a function of composition x. The values of k at the commensurate compositions of $x = 1.2$ and 1.33 were thereby found to be 0.6 and 0.6667, respectively. This k is related to the multiplicity m_M used by Mijlhoff et al. [13] via the relation $m_M = 2/(1-k)$ and to the Ba occupancy via $x = 2k$. This relationship was found to work well in the middle of the compositional range but to break down at either end. Cheary and Squadrito [19] thus proposed the formation of microdomains to help explain this variation at either end. The concept of microdomains is, however, unnecessary if the $Ba_xMg_xTi_{8-x}O_{16}$ hollandite is described as a composite modulated, single phase solid solution. We believe the Ba occupancies in $Ba_xMg_xTi_{8-x}O_{16}$ studied by Cheary and Squadrito [20] to be systematically underestimated at minimum x and overestimated at maximum x.

The only previously reported barium manganese titanate hollandite in the literature was that reported for $BaMnTi_5O_{12}$ by Prieto et al. [29]. They described it as a triple hollandite-type structure with $P2/n$ monoclinic space group. In this study, a single phase monoclinic hollandite solid solution was found with a composition range from $x = 1.168(2)$ to 1.234(2) (see Table 3).

Previous reports describing $Ba_xFe_{2x}Ti_{8-2x}O_{16}$ hollandites have reported composition ranges from 1.07 to 1.40 [20,31–34]. The lattice parameters we have obtained agree well with the literature values. Our solid solution range has a maximum x value of 1.350(2). The minimum x value is undetermined but less than 1.210(3) (see Table 4). No previous literature report on $Ba_xFe_xTi_{8-x}O_{16}$ hollandites, however, could be found at all. Our results give the maximum occupancy for $Ba_xFe_xTi_{8-x}O_{16}$ as $x = 1.309(2)$ while the minimum x value is less than 1.251(3) (see Table 4).

4.2. Other hollandite systems incorporating M^{3+} ions

Zandbergen et al. [8] have studied an extensive selection of $Ba_xM^{3+}_{2x}Ti_{8-2x}O_{16}$, M = Sc, Al, Ga and Cr, hollandites by means of both electron and X-ray diffraction. All were reported to exist over the same range of Ba content, i.e., $1.12 < x < 1.32$. They describe the transverse correlation between the phases of occupational waves (describing the Ba ordering in the tunnels) as strong when sharp satellite reflections are observed, intermediate when slight smearing of the satellite reflections (perpendicular to the tunnel axis) is observed or weak when diffuse sheets (perpendicular to the tunnel axis) are observed in EDPs (cf. with e.g., Figs. 2a and 3a). Zandbergen et al. [8] found this transverse correlation to be strong when M = Ga, strong to intermediate for M = Al and Cr and intermediate for M = Sc. The reported three-dimensional ordering of the Ba ions in the $Ba_xM_{2x}Ti_{8-2x}O_{16}$ systems for M = Sc, Al, Ga and Cr suggests that these hollandites also behave as composite modulated single phase solid solutions.

4.3. Hollandite systems incorporating monovalent A cations

In all reported studies on hollandites of $A_xM_yTi_{8-y}O_{16}$ where A = Cs, K and Rb and M = Sc, Al, Ga, Zn, Co, Mg, Fe^{3+}, Fe^{2+}, Mn^{2+} and Cr^{3+} (not all combinations have been studied) [7,35–40] three-dimensional ordering of the A cations has essentially been reduced to only one-dimensional ordering along the tunnel axis (see e.g., the $\langle 110 \rangle$ zone axis EDP of $Cs_{1.5}Zn_{0.75}Ti_{7.25}O_{16}$ (nominal composition) shown in Fig. 2a or the $\langle 010 \rangle$ zone axis EDP of the same Cs hollandite shown in Fig. 3b) with the originally sharp satellite spots on the EDPs becoming smeared out perpendicular to the tunnel axis direction and eventually giving rise to only diffuse sheets of intensity perpendicular to the tunnel axis direction (cf. e.g., Fig. 2a with Fig. 2b). The relationship between composition and the component of these diffuse sheets along the tunnel axis direction, $q = x/2$, however, remains even when the ordering is only one-dimensional. Thus diffuse sheets running perpendicular to $\mathbf{c}^*$ at $\sim \pm 0.72\ \mathbf{c}^*$ occur around both the I-centred allowed framework sub-structure parent reflections such as, e.g., 110 or 200 as well as around the I-centred forbidden framework sub-structure parent reflections such as, e.g., 001 (see Figs. 2a and 3a).

In the case of the fully (3 + 1)-d ordered hollandites, the former "satellite" would be forbidden by the superspace centering operation. This centering operation, however, is destroyed in the case of the 1-d ordered hollandites.

4.4. Factors controlling A site ordering in hollandites

Previous workers [10,12,41,42] have reported four factors as influencing A site ordering in $A_xB_8O_{16}$ ($1<x<2$) phases with hollandite-type structures. Firstly, electrostatic repulsion between tunnel cations within the same tunnel (intratunnel repulsion). Secondly, inter-tunnel interactions between A site cations in neighbouring tunnels. Thirdly, the shielding capacity of the octahedral framework and, finally, kinetic effects.

In early work, Bayer and Hoffman [40] synthesized titanate hollandites with all the potential tunnel sites of the framework occupied (corresponding to $x = 2$) when the tunnel, or A, cations were Rb or K. When the tunnel cations were Ba or a mixture of Ba and K, however, full occupancy was never obtained, i.e., x was always <2. Reid and Ringwood [41] noted similar trends in silicate hollandites where Sr or Ba aluminosilicates were found to have tunnel site occupancies of 75% (corresponding to $x = 1.5$). They suggested that this was probably due to a combination of overcrowding and increased electrostatic repulsion preventing complete filling of all available tunnel sites.

The above observations of Bayer and Hoffman [40] and Reid and Ringwood [41], in conjunction with subsequent work on hollandites [3,4,8,10–12,17–21], demonstrate that x is always <2 irrespective of the nature of the framework cations if some or all the tunnel cations are divalent and that the resultant hollandite materials commonly adopt fully ordered structures. If intra-tunnel interactions were the only factor responsible for ordering of A site tunnel ions in hollandites, and the framework sub-structure provided a perfect barrier between neighbouring tunnels, hollandites would be expected to only ever display one-dimensional ordering. Three-dimensional ordering, however, is commonplace in titanate hollandites (this work, [3,8,10-12,17–21]).

Barium titanate hollandites almost always adopt three-dimensional ordering of the tunnel ions. Bursill and Grzinic [10], e.g., found that $Ba_xMg_xTi_{8-x}O_{16}$ had well-developed three-dimensional ordering of the Ba ions whereas $K_xMg_{x/2}Ti_{8-x/2}O_{16}$ hollandite displayed only one-dimensional ordering. They attributed this to the higher charge density of the Ba^{2+} ions (compared to the K^+ ions) being strong enough to overcome the shielding of the octahedral framework sub-structure. Thus the charge densities and formal valences of the tunnel ions are clearly important in determining the extent of long-range ordering.

Kesson and White [11] argued that the inter-tunnel shielding provided by the octahedral framework should also be taken into account. They proposed that the capacity of the B_8O_{16} octahedral framework to inhibit the interactions between the tunnel cations is largely determined by the polarizing power of the B cations. (An explanation of polarizing power and octahedral shielding capacity and how to calculate them is

Table 5
Stoichiometry, octahedral shielding capacity, lattice parameters and degree ordering for a number of hollandites

Stoichiometry	Octahedral shielding capacity	Lattice parameters				Ordering	Reference
		a (Å)	b (Å)	c (Å)	β (°)		
$Ba_xZn_xTi_{8-x}O_{16}$, $x = 1.174$	2.09	10.219(1)	2.978(1)	9.989(1)	90.72(2)	3D	This work
$Ba_xCo_xTi_{8-x}O_{16}$, $x = 1.164$	2.08	10.200(1)	2.970(1)	10.005(1)	90.62(1)	3D	This work
$Ba_xMg_xTi_{8-x}O_{16}$, $x = 1.164$	2.08	10.178(1)	2.971(1)	10.010(1)	90.50(1)	3D	This work
$Ba_xMn_xTi_{8-x}O_{16}$, $x = 1.168$	2.10	10.279(1)	2.991(1)	10.001(1)	91.87(2)	3D	This work
$Ba_xFe_{2x}Ti_{8-2x}O_{16}$, $x\sim1$	2.25	10.103(1)		2.970(1)		3D[a]	This work
$Ba_xFe_{2x}Ti_{8-2x}O_{16}$, $x = 1.350$	2.40	10.247(1)	2.981(1)	9.906(1)	91·10(2)	3D	This work
$Ba_xFe_xTi_{8-x}O_{16}$, $x\sim1$	1.98	10.139(1)		2.971(1)		3D[a]	This work
$Ba_xFe_xTi_{8-x}O_{16}$, $x = 1.306$	2.00	10.287(1)	2.978(1)	9.933(1)	91·15(2)	3D	This work
$Ba_xAl_{2x}Ti_{8-2x}O_{16}$, $x = 1.28$	2.00	9.946(1)		2.923(1)		3D with slight smearing	8
$Ba_xGa_{2x}Ti_{8-2x}O_{16}$, $x = 1.32$	2.09	10.048(2)		2.961(1)		3D	8
$Ba_xCr_{2x}Ti_{8-2x}O_{16}$, $x = 1.32$	2.09	10.133(6)	9.871(7)	2.953(1)	90.87(3)	3D with slight smearing	8
$Ba_xRu_{2x}Ru_{8-2x}O_{16}$, $x = 1.36$	2.17	9.821(3)		3.121(1)		3D	8
$Ba_xCr_{2x}Sn_{8-2x}O_{16}$, $x = 1.38$	2.29	10.516(2)	3.104(2)	10.025(4)	91.47(1)	1D	8
$Ba_xSc_{2x}Sn_{8-2x}O_{16}$, $x = 1.44$	2.42	10.694(9)	3.193(4)	10.231(9)	92.10	3D with slight smearing	8
$Ba_xCr_{2x}Ge_{8-2x}O_{16}$, $x = 1.36$	1.88	9.800(3)		2.948(1)		1D	8
$Ba_xMo_{2x}Mo_{8-2x}O_{16}$, $x\sim1.143$	2.21	10.21		2.89		3D	16
$Ba_xTi_{2x}Ti_{8-2x}O_{16}$, $x = 1.14$	2.10	10.179	2.958	10.202	90.78[b]	3D /1D	11
$Ba_xCr_{2x}Ru_{8-2x}O_{16}$, $x = 1.30$	2.10	9.888(2)		3 × 3.0403 (2)[c]		3D	42

[a]Weak superlattice peaks in XRD patterns.
[b]Lattice parameters converted from $C2/m$ to $I2/m$.
[c]Tripling of c-axis.

presented in Ref. [11].) Table 5 lists the stoichiometry, octahedral shielding capacity, lattice parameters and degree of ordering for a number of hollandites in this study and others. The data in Table 5 show that the octahedral shielding capacity has little effect on the ordering of barium titanate hollandites. All known examples exhibit full three-dimensional ordering. The barium titanate hollandites containing Fe, Al and Cr each show some disorder (spots on the EDPs becoming smeared out perpendicular to the tunnel axis direction, XRD patterns show broad superlattice peaks) yet the octahedral shielding capacity is the lowest for Al and the highest for Fe in the barium titanate hollandites. The octahedral shielding capacity also does not seem to affect the degree of ordering in the non-titanate hollandites presented in Table 5.

On examining the data in Table 5, it would appear that the size of the octahedral framework sub-cell also has little to do with the extent of ordering although, in the case of the titanate hollandites, it appears that the monoclinic hollandites exhibit greater Ba ion ordering than the tetragonal hollandites. The work by Cheary et al. [20] showed the order–disorder transition from an *A* site 3-d ordered structure to a less-ordered structure occurred above the monoclinic–tetragonal transformation. There is also a general trend in the Ba titanate hollandites for the ones with the smallest *a* lattice parameters to be the least ordered.

Finally, kinetic effects must also be taken into consideration as is clear from the work of Cheary et al. [18] and this work (see $Ba_xFe_{2x}Ti_{8-2x}O_{16}$ above) in that the ordering of the Ba ions could clearly be enhanced by slowly cooling the hollandite. In this study we quenched selected hollandites to see if the three-dimensional ordering of the Ba ions could be removed (see above). Thus it is clear that the cooling rate is important in determining the degree of ordering of the *A* site cations. The critical cooling rate for maximum ordering also depends on the chemical composition of the hollandite. In this study the Fe^{3+}-containing hollandites required a slower cooling rate to maximize ordering by comparison with other hollandites.

5. Conclusions

Diffraction studies have confirmed that the $Ba_x^{2+}M_x^{2+}Ti_{8-x}^{4+}O_{16}$ (M = Zn, Co, Mg, Fe and Mn) and $Ba_x^{2+}M_{2x}^{3+}Ti_{8-2x}^{4+}O_{16}$ (M = Fe) barium hollandites studied are all composite modulated, single phase solid solutions made up of mutually incommensurable (along **b**) framework and Ba ion sub-structures. The overall superspace group symmetry was found to be $I2/m(0,\frac{x}{2},0)1$ in each case. Such a composite modulated structure approach to hollandite solid solution systems eliminates altogether the need for Ba/vacancy ordering (see e.g., Refs. [13,14]) and leads to a direct and necessary relationship between composition x and the reciprocal space positioning of satellite reflections. This relationship enables the solid solution composition ranges for the hollandites to be calculated directly from the positions of well-defined satellite peaks in X-ray diffraction patterns. The obtained solid solution ranges differ significantly for the various Ba hollandite systems although the Ba ion occupancy x was always found in the range from ~1.1 to ~1.3.

The underlying crystal chemistry responsible for this behaviour is not immediately apparent. Full (3 + 1)-d incommensurate composite modulated structure refinements, in particular of the displacive Atomic Modulation Function (or AMF) describing the deviation of the Ba ions in the tunnels away from their underlying Ba sub-structure positions as a function of $\mathbf{b}_f^*.(\mathbf{r}_{Ba}+\mathbf{t}_{Ba})$ (see e.g., Refs.[23–25]) for the various hollandite systems, may well provide additional insight. Note that a sawtooth-shaped displacive AMF (see e.g., Ref. [43]) is to be expected if the Ba ions turn out to prefer a specific location within the host octahedral framework sub-structure. If, however, their location is not so tightly prescribed, then a displacive AMF with a shape intermediate between a sawtooth and a flat line is to be expected. Refinement of sawtooth-shaped AMFs, however, is not a trivial matter. Note also that knowledge of the overall superspace group symmetry constrains the shape of these displacive AMFs as well as the symmetry relationship between the AMFs of the two Ba ions per Ba ion sub-structure.

The ordering of Ba ions can clearly be enhanced by slow cooling of the hollandite or diminished by quenching. The critical cooling rate for maximum ordering of Ba ions was found to be dependent upon the chemical composition of the hollandite. The size of the framework sub-cell in Ba titanate hollandites was also found to have some effect on the extent of ordering of the Ba ions in that the monoclinic hollandites exhibit greater Ba ion ordering than the tetragonal hollandites.

Acknowledgments

The authors wish to acknowledge Ben Teale, Mugdha Bhati and Joel Davis for their assistance in the preparation and SEM examination of the samples in this study. RLW thanks the Australian Research Council (ARC) for financial assistance in the form on an ARC Discovery Grant.

References

[1] A. Byström, A.M. Byström, Acta Crystallogr. 3 (1950) 146–154.
[2] R.W. Cheary, Acta Crystallogr. B 42 (1986) 229–236.

[3] J.E. Post, R.B. Von Dreele, P.R. Buseck, Acta. Crystallogr. B 38 (1982) 1056–1065.
[4] R.D. Shannon, Acta. Crystallogr. B 32 (1976) 751–767.
[5] J.S. Dryden, A.D. Wadsley, Trans. Faraday Soc. 54 (1958) 1574–1580.
[6] B. Mukherjee, Acta Crystallogr. 17 (1964) 1325–1326.
[7] H.U. Beyeler, Phys. Rev. Lett. 37 (1976) 1557–1560.
[8] H.W. Zandbergen, P.L.A. Everstijn, F.C. Mijlhoff, G.H. Renees, D.J.W. IJdo, Mater. Res. Bull. 22 (1987) 431–438.
[9] J.R. Plaisier, A.A.C. van Vliet, D.J.W. IJdo, J. Alloys Compd. 314 (2001) 56–61.
[10] L.A. Bursill, G. Grzinic, Acta Crystallogr. B 36 (1980) 2902–2913.
[11] S.E. Kesson, T.J. White, Proc. R. Soc. London Ser. A 405 (1986) 73–101.
[12] S.E. Kesson, T.J. White, Proc. R. Soc. London Ser. A 408 (1986) 295–319.
[13] F.C. Mijlhoff, D.J.W. IJdo, H.W. Zandbergen, Acta Crystallogr. B 41 (1985) 98–101.
[14] E. Fanchon, J. Vicat, J.-L. Hodeau, P. Wolfers, D.T. Qui, P. Strobel, Acta Crystallogr. B 43 (1987) 440–448.
[15] X.J. Wu, F.H. Li, Acta. Crystallogr. B 46 (1990) 111–117.
[16] N. Barrier, P. Gougeon, R. Retoux, J. Alloys Compd. 317–318 (2001) 120–126.
[17] L.A. Bursill, J. Kwiatkowska, J. Solid State Chem. 52 (1984) 45–52.
[18] R.W. Cheary, Mater. Sci. Forum 27/28 (1988) 397–406.
[19] R.W. Cheary, R. Squadrito, Acta Crystallogr. A 48 (1992) 15–27.
[20] R.W. Cheary, R. Squadrito, Acta Crystallogr. B 45 (1989) 205–212.
[21] R.W. Cheary, R. Thompson, P. Watson, Mater. Sci. Forum 228–231 (1996) 777–782.
[22] M.L. Carter, R.L. Withers, Z. Kristallogr. 219 (2004) 763–767.
[23] S. van Smaalen, Cryst. Rev. 4 (1995) 79–202.
[24] R.L. Withers, S. Schmid, J.G. Thompson, Prog. Solid State Chem. 26 (1998) 1–96.
[25] T. Janssen, A. Janner, A. Looijenga-Vos, P.M. de Wolff, in: A.J. Wilson (Ed.), International Tables for Crystallography, vol. C, Kluwer Academic Publishers, Dordrecht, 1992, pp. 797–835.
[26] M.L. Carter, E.R. Vance, D.R.G. Mitchell, Z. Zhang, in: J.M. Hanchar, S. Stroes-Gascoyne, L. Browning (Eds.), Scientific Basis for Nuclear Waste Management XXVIII, Materials Research Society, Warrendale, PA, USA, 2004, p. 249.
[27] A.E. Ringwood, S.E. Kesson, K.D. Reeve, D.M. Levins, E.J. Ramm, in: W. Lutze, R.C. Ewing (Eds.), Radioactive Waste Forms for the Future, North-Holland, New York, 1988, p. 233.
[28] R.S. Roth, C.J. Rawm, C.G. Lindsay, W. Wong-Ng, J. Solid State Chem. 104 (1993) 99–118.
[29] A.L. Prieto, T. Siegrist, L.F. Schneemeyer, Solid State Sci. 4 (2002) 323–327.
[30] M.L. Carter, Mater. Res. Bull. 39 (7–8) (2004) 1075–1081.
[31] M.C. Cadee, G.C. Verschoor, Acta. Crystallogr. B 34 (1978) 3554–3558.
[32] T.A. Vanderah, J.M. Loezos, R.S. Roth, J. Solid State Chem. 121 (1996) 38–50.
[33] J.M. Loezos, T.A. Vanderah, A.R. Drews, Powder Diffrac. 14 (1999) 31–35.
[34] H. Trauchi, T. Futamura, T. Ishii, Y. Fujiki, J. Phys. Soc. Japan 53 (7) (1984) 2311–2315.
[35] H.U. Beyeler, C. Schüler, Solid State Ionics 1 (1980) 77–86.
[36] L.F. Grigor'eva, S.A. Petrov, V.P. Popov, D.P. Romanov, Neorg. Mater. 22 (1984) 631–635.
[37] Y. Onoda, Y. Fujiki, S. Yoshikado, T. Ohachi, I. Taniguchi, Solid State Ionics 18 and 19 (1986) 878–882.
[38] R.W. Cheary, Acta. Crystallogr. B 43 (1987) 28–34.
[39] S.A. Petrov, L.F. Grigor'eva, I.Yu. Sazeev, S.K. Filatov, Inorgan. Mater. 307 (1994) 892–895.
[40] G. Bayer, W. Hoffmann, Am. Miner. 51 (1966) 511–516.
[41] A.F. Reid, A.E. Ringwood, J. Solid State Chem. 1 (1969) 6–9.
[42] M.C. Cadee, A. Prodan, Mater. Res. Bull. 14 (1979) 613–618.
[43] L. Elcoro, J.M. Perez-Mato, R. Withers, Z. Kristallogr. 215 (2000) 727–739.